This is the final draft of the contribution published as:

Shan, Y., Qin, J., Harms, H., Wick, L.Y. (2020):
Electrokinetic effects on the interaction of phenanthrene with geo-sorbents
Chemosphere **242** , art. 125161

The publisher's version is available at:

http://dx.doi.org/10.1016/j.chemosphere.2019.125161

ELECTROKINETIC EFFECTS ON THE INTERACTION OF PHENANTHRENE WITH GEO-SORBENTS

Yongping Shan[1§], Jinyi Qin[1,§#], Hauke Harms[1], Lukas Y. Wick[1]*

[1] *UFZ - Helmholtz Centre for Environmental Research, Department of Environmental Microbiology, 04318 Leipzig, Germany;*
[#] *present address: School of Civil Engineering, Chang'an University, Xi'an 710054, P.R. China*

Running title: Electrokinetic effects on the interaction of phenanthrene with geo-sorbents

Intended for: Chemosphere

[*] Corresponding author: Mailing address: Helmholtz Centre for Environmental Research - UFZ. Department of Environmental Microbiology; Permoserstrasse 15; 04318 Leipzig, Germany. phone: +49 341 235 1316, fax: +49 341 235 1351, e-mail: lukas.wick@ufz.de.
[§] both authors contributed equally to the manuscript.

ABSTRACT

Interactions with solid matrices control the persistence and (bio-)degradability of hydrophobic organic chemicals (HOC). Approaches influencing the rate or extent of HOC interactions with matrices are thus longed for. When a direct current (DC) electric field is applied to a matrix immersed in an ionic solution, it invokes transport processes including electromigration, electrophoresis, and electroosmotic flow (EOF). EOF is the surface charge-induced movement of pore fluids. It has the potential to mobilize uncharged organic contaminants and, hence, to influence their interactions with sorbing geo-matrices (i.e. geo-sorbents). Here, we assessed the effects of weak DC electric fields on sorption and desorption of phenanthrene (PHE) in various mineral and carbonaceous geo-sorbents. We found that DC fields significantly changed the rates and extent of PHE sorption and desorption as compared to DC-free controls. A distinct correlation between the Gibbs free energy change (ΔG^o) and electrokinetic effects such as the EOF velocity was observed; in case of mineral sorbents EOF limited (or even inhibited) PHE sorption and increased its desorption. In strongly sorbing carbonaceous geo-sorbents, however, EOF significantly increased the rates of PHE sorption and reduced PHE desorption by > 99 % for both activated charcoal and exfoliated graphite. Based on our findings, an approach linking ΔG^o and EOF velocity was developed to estimate DC-induced PHE sorption and desorption benefits on mineral and carbonaceous sorbents. We conclude that such kinetic regulation gives rise to future technical applications that may allow modulating sorption processes e.g. in response to fluctuating sorbate concentrations in contaminated water streams.

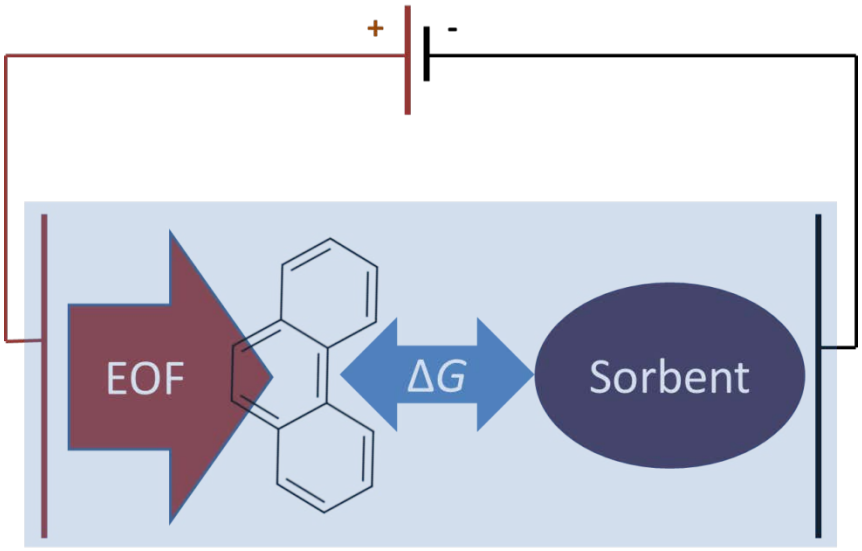
KEY WORDS:

Phenanthrene, electrokinetics, electroosmotic flow, sorption thermodynamics

BRIEF

DC electric fields significantly influence the rates and extents of sorption and desorption of phenanthrene to mineral and carbonaceous model geo-sorbents by electroosmotic flow.

ABSTRACT ART



1. INTRODUCTION

Interactions with solid geo-matrices are key drivers of the persistence of hydrophobic organic chemicals (HOC) and, hence, control their fate as well as the exposure of environmental and human receptors (Harms et al., 2017b). Various studies have shown that the sequestration of hydrophobic chemicals in the solid phase significantly reduces HOC bioavailability and biodegradation (Harms et al., 2017a). Three potentially rate-limiting steps may influence the sorption of a chemical to and its release from geo-matrices, respectively: (i) diffusion of the chemical within the molecular nano-porous network, (ii) pore or surface diffusion in aggregated geo-matrices, and (iii) diffusion of the sorbate across an aqueous boundary layer surrounding sorbent particles. As a consequence of progressive binding, residual hydrophobic chemical may become less leachable and thus less efficiently available for microbial degradation (Johnsen et al., 2005). The sorption and release of HOC in various sorbents can be investigated by kinetic (Ahn et al., 2005; Ho et al., 2000; Morelis and van Noort, 2008) and thermodynamic (e.g., Gibbs free energy of sorption, ΔG^{o}) approaches (Doke and Khan, 2013; Huang and Weber, 1997). Electrokinetic approaches (Qin et al., 2015a, 2015b; Shan et al., 2018) (typically using DC fields of an electric field strength of X = 0.2 - 2.0 V cm^{-1}) have shown high potential to mobilize otherwise poorly mobilizable hydrophobic organic pollutants in matrices of low permeability (Jeon et al., 2010; Kim et al., 2006; Li et al., 2000; Pham et al., 2009; Reddy, 2010; Saichek and Reddy, 2003; Shaplro and Probstein, 1993). When an electric field is applied to a matrix immersed in an ionic solution, it invokes transport processes including electromigration, electrophoresis, and electroosmotic flow (EOF). Electromigration and electrophoresis refer to the transport of charged molecules and particles to electrodes of opposite charge. EOF is the surface charge-induced movement of pore fluids in an electric field usually moving from the anode toward the cathode (Rice

and Whitehead, 1965). It originates from the enrichment of ions in the so-called electric double layer near a surface and is particularly effective in fine-grained materials where meso- and micro-pores dominate. These are situations where low hydraulic flow is extremely small and molecular diffusion may limit the access of sorbates to and the release of sorbates from smaller pores(Reddy and Saichek, 2004; Shi et al., 2008). Electroosmotic perfusion induces efficient liquid flow in inter- and intra-particle network pore channels (Tallarek et al., 2001) and, hence, increase release rates and natural attenuation of HOC at locations where pump and treat approaches may be inadequate (Kim et al., 2007; Reddy et al., 2009; Reddy and Saichek, 2004) or energetically ineffective (Hassan et al., 2015). EOF can thus be applied for the dispersal and separation of uncharged entities or the dewatering of matrices (Hoshyargar et al., 2018; Li et al., 2018). Contrary to the parabolic velocity profile of pressure-driven hydraulic flow in a pore, the velocity profile of EOF is quasi planar beginning at the so-called electrical double layer located a few nanometers above the surface. It thus likely arises at scales relevant for chemical-sorbent interactions. This effect is, for instance, used in capillary electrochromatography (CEC) where EOF (rather than pressure-driven-flow such as in HPLC) is used to effectively separate uncharged solutes between a mobile and a stationary phase (Vallano and Remcho, 2000). Recent work showed that DC fields increased PHE sorption rates in carbonaceous exfoliated graphite sevenfold and reduced the PHE desorption rate by > 99 % (Qin et al., 2015a). This was discussed as a result of electroosmotic perfusion of PHE to pores that contribute most of the sorption sites, but are difficult to access in the absence of EOF by molecular diffusion only. Still scarce mechanistic information exists on the impact of DC on the sorption and desorption of hydrophobic chemicals with geo-matrices. In our study we tested whether electrokinetic phenomena are able to change interactions of the common oil contaminant (Bansal and Kim, 2015) phenanthrene (PHE)

with mineral (zeolites, aluminum oxides, silicates) and carbonaceous (activated charcoal, exfoliated graphite) sorbents as compared to DC-free controls. In particular, we assessed to which degree (i) DC electric fields influence the sorption and desorption of PHE in model sorbents of differing sorption strength, (ii) DC-induced benefits of PHE sorption/desorption correlate with Gibbs free enthalpy (ΔG^{o}), and (iii) EOF may explain DC-induced benefits of PHE-geo-matrix interactions.

2. MATERIAL AND METHODS

2.1 Reagents and sorbents.

One hundred mg PHE (purum > 97.0 % GC; Fluka, Germany) were stirred in 100 mL of methanol in a light-protected volumetric flask for one hour. One mL of the methanolic PHE solution was then added to 1 L of either a sterile 1, 10 or 100 mmol L^{-1} potassium phosphate buffer (PB; i.e. K_2HPO_4, KH_2PO_4) at pH = 7, shaken for 24 h under light exclusion and stored at 4 °C until use. Except for the exfoliated graphite (EG), which was prepared as described earlier,(Moustafa, 2009; Qin et al., 2015a) all sorbents (silica gel 40Å, 60Å, 100Å (Davisil), aluminum oxide (Al_2O_3; Si/Al = 0), Zeolite NaY (Si/Al = 5), Zeolite 13X (Si/Al = 1.4) and activated charcoal (AC)) were purchased from Sigma-Aldrich Chemie GmbH, Germany. The mineral sorbents were cleaned by exposure to 500 ˚C for 4 h in a muffle furnace and subsequent storage in a desiccator. For desorption experiments the sorbents were spiked with PHE as described earlier (Puglisi et al., 2007); shortly, 10 mg of the sorbents were added to 10 mL of hexane containing 1 mg mL^{-1} of PHE in a tightly sealed vial and sonicated for one h in an ultrasonic bath (Sonorex Super RK255/H, Bandelin Electronic GmbH). Thereafter, the vial was opened and the hexane allowed evaporating at 60 ˚C for 10 min. After loading, all of the sorbents were stored at 5 ˚C in a closed vial in the dark.

2.2 Analytical methods.

Aqueous samples with dissolved PHE were analyzed by high performance liquid chromatography (HPLC) (Shimadzu Class-VP) on an RP-18 column (Nucleosil 100-5 C18 4 mm ID) using an isocratic mobile phase (MeOH / water (90:10 v/v); flow: 1 mL min^{-1}) and UV detection at 250 nm. The physicochemical surface characteristics (BET surface, pore size

and the zeta potential (ζ)) of the sorbents were characterized by Doppler electrophoretic light scattering analysis, and BET analysis (cf. Figure S1).

2.3 Electrokinetic apparatus and running conditions.

The electrokinetic apparatus used for the sorption and desorption was composed of two electrode compartments and three central chambers. (cf. Figure S2) as described earlier by Qin et al. (Qin et al., 2015a). The apparatus was mounted horizontally, filled with either 1, 10, 50, or 100 mmol L^{-1} electrolyte, and connected to a PowerPac (P333, Szczecin, Poland) to produce an electric field of an electric field strength X of 1.8 V cm^{-1} and resulting currents I of 3 ± 0.4, 14 ± 2, 30 ± 3 mA for 1, 10, and 100 mmol L^{-1} of electrolyte, respectively. The electrolyte was circulated from the anode to the cathode by a peristaltic pump (ISM 935, Ismatec, Glattbrugg, Switzerland) with sterilized Teflon at 26.4 ml h^{-1} (bed flow velocity: 0.004 cm s^{-1}). Experiments in the absence of electric field were conducted as controls.

2.4 Kinetics of PHE Geo-sorbent Interactions

2.4.1 Desorption: Desorption of PHE from PHE-loaded sorbents was quantified in presence and absence of a DC electric field (X = 1.8 V cm^{-1}) in 10, 50 and 100 mmol L^{-1} electrolyte solutions. The central of the three chambers (cf. Figure S2) was packed with dry, PHE-spiked sorbent prepared as described by (Puglisi et al., 2007); either 1 g of a mineral sorbent (silica 40Å, 60Å, 100Å, Al_2O_3, zeolite NaY, zeolite 13X), 0.5 g of AC, or 70 mg of EG. The apparatus then was filled with 200 mL PB solution (denoted as t = 0 h) and continuously flushed overnight (11 h) for system equilibration prior to the application of the DC electric field. Thereafter samples of 1 mL were taken from chamber (3) (cf. Figure S2), transferred each to 1.5 mL glass vials and the PHE content analyzed by HPLC. No significant changes

of the temperature and the pH of the electrolyte were observed in either of the ionic strengths of the electrolyte used. All experiments were performed in three independent replicates.

2.4.2 Sorption. Sorption of PHE to sorbents was quantified in presence and absence of a DC electric field (X = 1.8 V cm^{-1}) in 1, 10 and 100 mmol L^{-1} electrolyte solutions. The chamber (4) (cf. Figure S2) was packed with dry, cleaned sorbent as described above, the apparatus was filled with 200 mL electrolyte solution and then continuously flushed with PHE containing electrolyte (C_e = 400 µg L^{-1}) at a rate of 26.4 mL h^{-1} under DC and DC-free conditions. After a stabilization time of 5 min (denoted as t = 0 h), samples of 1 mL were taken at given intervals from both chambers (1) and (3) next to the central chamber (4); (cf. Figure S2), transferred to 1.5 mL glass vials and the PHE contents were analyzed by HPLC. All experiments were performed in three independent replicates.

2.5 Determination of sorption isotherms.

Triplicate batch experiments of PHE sorption on all sorbents were performed separately either at 5 ± 2 °C, 25 ± 2 °C, and 35 ± 2 °C in 10 and 100 mmol L^{-1} PB. Isothermal sorption experiments were performed according to a standard protocol (Huang and Weber, 1997; Su et al., 2006; Zhao et al., 2014) in 30 mL (mineral sorbents) or 200 mL (carbonaceous sorbents) glass vials that were sealed with a Teflon-coated butyl rubber septum crimp cap. Activated charcoal was ground into fine particles (diameter 14 ± 3 µm, n = 20) to shorten the time needed to reach sorption equilibrium (James et al., 2005). The solid-to-solution ratios (w/v) were 1:20 (g mL^{-1}) for PHE sorption to mineral sorbents and 1:8000 (g mL^{-1}) for carbonaceous sorbents, respectively. Dissolved PHE concentrations of 100, 200, 300, 400, and 500 µg L^{-1} were used for mineral sorbent while 10, 20, 30, 40, 50, 60, 70, and 80 mg L^{-1}

were used for carbonaceous sorbents (0.1%, 0.2%, 0.3%, 0.4%, 0.5%, 0.6%, 0.7%, and 0.8% MeOH was added as co-solvent accordingly). The glass vials were horizontally shaken in a reciprocal shaker (3016, GFL, Germany) at 12 rpm for 7 days. All experiments were performed in three independent replicates. Aqueous PHE concentrations were quantified by HPLC as mentioned above. Sorption isotherms were approximated using Freundlich adsorption isotherm (eq. 1) (Ai and Jiang, 2012; Duan and Naidu, 2013; Zhang et al., 2010).

$$\log q_e = \log K_F + n \log C_e \qquad \text{(eq. 1)}$$

where q_e is the equilibrium concentration of PHE adsorbed to sorbents, C_e is the dissolved PHE equilibrium concentration, n is the Freundlich exponent (a measure of sorption linearity) and K_F is the Freundlich isotherm constant (μg kg^{-1}) (L μg^{-1})^n. The distribution coefficient K_d at equilibrium was determined by $K_d = q_e/C_e$ (L g^{-1}). The specific surface-normalized distribution coefficient K_d^* can be further calculated by dividing K_d by the specific surface area (m^2 g^{-1}) of the sorbents.

2.6 Calculation of sorbed and desorbed PHE fractions.

$\Gamma_{des,t}$ (%) and $\Gamma_{sor,t}$ (%) refer to normalized time-dependent fractions of PHE in the sorbent in desorption and sorption experiments, respectively. They were calculated from PHE inflow (C_i) and outflow concentrations (C_e) of the reactor chamber, the electrolyte volume flushed (V; L), and the initial PHE load (M_0; mg) in the sorbent and the maximum amount of PHE that can be loaded on clean sorbent in the column (M_s; mg), respectively (eqs. 2 & 3)

$$\Gamma_{des,t} = \frac{M_0 - \int_0^t C_e \, dV}{M_0} \qquad \text{(eq. 2)}$$

$$\Gamma_{sor,t} = \frac{\int_0^t C_i \, dV - \int_0^t C_e \, dV}{M_s} \qquad \text{(eq. 3)}$$

The relative influence of DC electric fields on PHE desorption ($\Delta\Gamma_{des,t}$) and sorption ($\Delta\Gamma_{sor,t}$) at a given time can be calculated from eqs. 4 & 5, where subscripts denote the absence and presence of the electric field.

$$\Delta\Gamma_{des,t} = \Gamma_{des,noDC,t} - \Gamma_{des,DC,t} \quad \text{(eq. 4)}$$

$$\Delta\Gamma_{sor,t} = \Gamma_{sor,noDC,t} - \Gamma_{sor,DC,t} \quad \text{(eq. 5)}$$

2.7 Thermodynamics of PHE geo-sorbent interactions.

The standard Gibbs free energy of sorption (ΔG^o) relates to standard sorption enthalpy (ΔH^o) and sorption entropy changes (ΔS^o) by eq. 6.

$$\Delta G^\circ = \Delta H^\circ - T\Delta S^\circ \quad \text{(eq. 6)}$$

ΔG^o can be estimated according to the following equation at T = 298 K:

$$\Delta G^\circ = -RT \ln K_c \quad \text{(eq. 7)}$$

K_c is the equilibrium constant; it is dimensionless and based on the Freundlich isotherm K_F (at 298 K) and the water density (ϱ) 1000 g L^{-1}, and can be calculated using eq. 8 (Ghosal and Gupta, 2015; Kopinke et al., 2018; Tran et al., 2017):

$$K_c = \frac{K_F \rho}{1000}\left(\frac{10^6}{\rho}\right)^{(1-n)} \quad \text{(eq. 8)}$$

ΔH can be estimated using the van't Hoff equation by substituting eq. 7 to eq. 6 (Kopinke et al., 2018; Tran et al., 2017):

$$\ln K_c = \frac{-\Delta H^\circ}{R} \times \frac{1}{T} + \frac{\Delta S^\circ}{R} \quad \text{(eq. 9)}$$

The ΔH^o (kJ mol^{-1}) is a measure of the enthalpy change (isosteric heat) involved in the transfer of solute from the reference state to the sorbed state at a given solid-phase concentration. R is the universal gas constant (8.314×10^{-3} kJ mol^{-1} K^{-1}) and T is temperature in Kelvin. The values of ΔH^o can be estimated by the slope and intercept of a plot of ln K_c versus 1/T, and ΔS^o can be calculated by ΔH^o and ΔG^o according to eq.6.

2.8 Approximation of the EOF velocity.

The electroosmotic (EOF) flow velocity in an intra-particle pore of radius r ($V_{EOF,r}$) can be calculated by $V_{EOF,\ max}$ and a function of κr (*i.e., f(κr)*) (Rice and Whitehead, 1965) as detailed by eqs. 10-12.

$$V_{EOF,r} = V_{EOF,max} * f(\kappa r) \quad \text{(eq. 10)}$$

$$V_{EOF,\ max} = -\frac{\varepsilon_r \cdot \varepsilon_0 \cdot X \cdot \zeta}{\eta} \quad \text{(eq. 11)}$$

$$f(\kappa r) = \left(1 - \frac{2I_1(\kappa r)}{\kappa r I_0(\kappa r)}\right) \quad \text{(eq. 12)}$$

Here I_0, I_1 are the zero and first-order modified Bessel functions, κ^{-1} the thickness of the electrical double layer (EDL, nm) calculated by the Guoy-Chapman theory with C and z the molar bulk concentration and the charge number of the electrolytes, respectively (Sharma and Rao, 2003) (eq. 13).

$$\kappa^{-1} = \left[3.29 z C^{1/2}\right]^{-1} \quad \text{(eq. 13)}$$

The term κr reflects the ratio of the pore radius (r) to the thickness of the double layer. Equation 10 is a simplified expression of the Navier-Stokes equation (Cummings et al., 2000), where, ε_r is the dielectric constant of water (78.5), ε_0 (8.85×10^{-12} F m^{-1}) is the vacuum permittivity, ζ is the actual zeta potential of the solid surface at the experimental conditions, and X is the electric field strength applied.

3. RESULTS

3.1 Characterization of sorbent properties

Physico-chemical properties including specific surface area, average pore size, and zeta potential were analyzed for all eight sorbents (Table 1). All sorbents had average pore sizes of 2-10 nm and were of a high specific surface area (> 190 $m^2 g^{-1}$), with AC, EG, silica 40Å and zeolite 13X expressing specific surface area > 500 $m^2 g^{-1}$. Although the carbonaceous materials had lower charges, all sorbents exhibited clearly negative zeta potentials at all ionic strengths tested (Table 1). Silica 40 Å, silica 60 Å, and silica 100 Å exhibited similar zeta potentials in all the electrolyte concentrations. The equilibrium sorption capacities were reflected by the surface normalized partition coefficients K_d^* ranging from 1×10^{-6} mL cm^{-2} (mineral sorbents) to 0.148×10^{-3} mL cm^{-2} for carbonaceous sorbents. Minor effects of the ionic strength on K_d^* for 10 mmol L^{-1} and 100 mmol L^{-1} at 25 °C were found (Table 1).

3.2 Effect of the DC field on PHE-sorbent interactions

In order to assess the effect of weak DC electric fields on PHE-sorbent interactions, all sorbents were exposed to a DC electric field of X = 1.8 V cm^{-1} at fixed bed conditions and the extent and the rates of PHE sorption and desorption compared to DC-free controls. Clear DC-field effects on both PHE sorption and desorption were observed as evidenced by time dependent relative PHE fractions remaining in the sorbents in desorption $\Gamma_{des,t}$ (%) and sorption $\Gamma_{sor,t}$ (%) experiments (Figures 1 & S3). In mineral sorbents the DC field stimulated the PHE desorption (Figures 1A & C) and reduced the extent of PHE sorption by 30-40 % (Figures 1B & D). By contrast, in carbonaceous EG and AC, DC field treatment increased PHE sorption (Figures 1F & H), and limited PHE desorption from EG (Figure 1E). No PHE release from AC was observed at any condition (Figure 1G). As EOF velocity depends on the ionic strength of the electrolyte, PHE desorption and sorption experiments further evaluated the effect of different electrolyte ionic strengths (1, 10, 100 mmol L^{-1} PB in sorption

experiments and 10, 50, 100 mmol L^{-1} PB in desorption experiments). As the electrolyte ionic strengths also may influence the sorption properties in the absence of DC, we calculated the effects of DC electric fields on PHE desorption ($\Delta\Gamma_{des,t}$) and sorption ($\Delta\Gamma_{sor,t}$) relative to DC free controls. Positive $\Delta\Gamma_{des,t}$ refers to increased desorption in presence of DC, while a negative $\Delta\Gamma_{des,t}$ refers to reduced desorption. Similarly, positive $\Delta\Gamma_{sor,t}$ denotes decreased sorption to the geo-sorbents relative to the control, while negative values refer to increased sorption. Figure 2 depicts $\Delta\Gamma_{des,t}$ and $\Delta\Gamma_{sor,t}$ for two mineral (silica 40Å, Zeolite NaY) and two carbonaceous (AC, EG) materials exposed to various electrolyte ionic strengths: at low (1 mM) electrolyte concentrations the DC electric field showed minor or no significant change of $\Gamma_{sor,t}$ and, hence minor DC effects on PHE sorption (Figures 2 & S4) while an increase of the electrolyte ionic strength resulted in $\Delta\Gamma_{sor,t} > 0$ (i.e., reduced sorption, Figures 2B & D) for mineral and $\Delta\Gamma_{sor,t} < 0$ (i.e., increased sorption, Figures 2F & H) for carbonaceous materials. Likewise electrolyte effects on DC-induced PHE desorption from mineral sorbents were observed: increased ionic strength resulted in improved PHE desorption ($\Delta\Gamma_{des,t} > 0$) for silica 40Å and Zeolite NaY (Figures 2A & C), yet had no apparent impact in AC (($\Delta\Gamma_{des,t} \approx 0$) Figure 2E).

4. DISCUSSION

4.1 Effects of the DC field on PHE-sorption and desorption kinetics

Applying a DC field to a suspended solid matrix invokes electrokinetic effects such as EOF, resulting from the motion of mobile counter-ions in the EDL located at the walls of pores and continuous micro-channels (Sinton and Li, 2003; Tallarek et al., 2001). As EOF exerts a dispersive force on PHE molecules while acting at scales relevant for chemical-sorbent

interactions, we quantified electrokinetic impacts on the sorption and desorption kinetics of PHE using zeolites, aluminum oxides, silicates, activated carbon and exfoliated graphite. These model geo-sorbents cover a broad range of physicochemical and morphological properties as well as PHE sorption characteristics (Table 1). Suspended sorbents were exposed in a fixed-bed reactor to a weak DC field and differing electrolyte concentrations at constant hydraulic flow. The rates of PHE sorption and desorption were then compared to those in identical DC-free controls. As the EOF velocity ($V_{EOF,r}$; eq. 10) is directly proportional to $f(\kappa r)$ and ζ; representing two distinct sorbent properties, we presumed that increasing $V_{EOF,r}$ would influence PHE sorption to and PHE desorption from sorption sites beyond mere mass diffusion. Figures 3C & D correlate observed relative benefits of DC electric fields on PHE desorption ($\Delta\Gamma_{des,t=86h}$) and sorption ($\Delta\Gamma_{sor,t=31h}$) to the calculated $V_{EOF,r}$ (Fig 3C & D), and the logarithmic surface-normalized PHE partition coefficient (Log K_d^*, Figures 3A&B) at the end of our experiments (i.e. at 86 h (desorption) and 31 h (sorption). Except for K_d that reflects equilibrium conditions, good correlations (R^2 = 0.90 for sorption at 31 h and 0.72 for desorption at 86 h) were detected, supporting the hypothesized effect of EOF on PHE-sorbent interaction (Figures 3C & D). In order to further evaluate DC-induced kinetic effects we varied the EDL thickness above the sorbents by changing electrolyte concentrations. A shift from 1 to 100 mmol L^{-1} results in a calculated reduction of the EDL thickness from 2.2 to 0.7 nm and an increase of the electroosmotic (EOF) flow velocity in ($V_{EOF,r}$). Simultaneously, a combination of bigger pores and smaller EDL thickness (i.e., increased κr, (eq. 10)) promotes an up to fivefold faster $V_{EOF,r}$ and proportional changes $\Delta\Gamma_{des,t}$, and $\Delta\Gamma_{sor,t}$ (Figure S6) for silica 40Å, 60Å, and 100 Å in PB electrolytes of varying ionic strengths. At conditions of low $V_{EOF,r;}$ (e.g. when the ionic strength of the electrolyte and/or the zeta potential of the sorbent is low) the DC field-induced impact on PHE-sorbent

interactions was low. For the strong PHE sorbents AC and EG, however, no correlation with K_d^*, and $V_{EOF,r}$ was observed (Figure 3). This suggests that the sorption properties of AC and EG for PHE prevail over the possible EOF effects. As better sorption of PHE to EG in presence of DC was observed, it may be speculated whether EOF may mediate the redistribution of weakly bound PHE within the sorbent (Ai and Jiang, 2012), i.e., translocate PHE molecules from weak to strong sorption sites.

4.2 Sorption thermodynamics and electrokinetic phenomena

In order to further interpret electrokinetic effects on PHE-sorbent interactions, we determined the changes of the Gibbs free energy (ΔG^o), the enthalpy (ΔH^o) and the entropy (ΔS^o) of PHE sorption to all sorbents (Table 2). ΔG^o is an indicator for the degree of spontaneity of PHE interaction with sorbents (Liu, 2009). A negative value ($\Delta G^o < 0$) thereby refers to a spontaneous reaction. ΔG^o of PHE sorption was found to be negative for all sorbents and poorly depended on the ionic strength of the PB electrolyte (Table 2). PHE sorption was exothermic ($\Delta H^o < 0$) and accompanied by minor changes of ΔS^o (Table 2). This observation confirms earlier work showing that hydrophobic (carbonaceous) and hydrophilic (mineral) surfaces exhibit distinct PAH sorption enthalpies in aqueous solutions (Drost-Hansen, 1978; Huang and Weber, 1997). As the interaction energy of water with mineral surfaces is greater than that of PAH, the water molecules may outcompete PAH molecules in an exothermic sorption processes. According to this assumption, PAH molecules may associate with a ~100 nm thick layer (Drost-Hansen, 1978) of vicinal water rather than directly with the mineral surface (Mader et al., 1997) and, hence, may be subject to significant EOF velocity. The plug-like velocity profile of EOF thereby is likely to exert a dispersing force on PHE molecules above mineral surfaces with a typical electric double layer thickness ranging from

0.65 nm to 6.87 nm for our experimental range of electrolyte concentrations (cf. eq. 13). According to the model postulated by Huang et al. (Huang and Weber, 1997), the PHE molecules are likely to interact directly with the surface of carbonaceous sorbents (i.e. express clearly negative ΔG^o) and hence may require a high EOF kinetic energy for being replaced by water molecules. Based on such reasoning, we tested whether there is an apparent correlation between $V_{EOF,r}$ and the Gibbs free energy for PHE molecule in the vicinity of a sorbent surface (Figure 4). Such *ad hoc* correlation is further tempting as the ionic strength of the electrolyte was found to have minor influence on ΔG^o yet to promote the intra-pore $V_{EOF,r}$. Figures 4 & S5 show that $V_{EOF,r}$ as low as 4.4×10^{-7} m s^{-1} result in significant sorption and desorption benefits for sorbents with ΔG^o > -13.5 kJ mol^{-1}. Generally, more negative ΔG^o and a lower EOF velocity seem to result in an electrokinetic promotion of PHE sorption (cf. warm color area in Figure 4B) and a reduction of PHE desorption (cf. cold color area in Figure 4A). By contrast, less negative ΔG^o and higher EOF may lead to electrokinetic promotion of PHE desorption (cf. warm color peaks in Figure 4A) and clearly reduced sorption (cf. cold color peaks in Figure 4B), respectively.

4.3 Conclusion: Relevance for environmental and biotechnological applications

The transformation of chemicals in natural and man-made systems is often mass transfer-limited as it requires chemicals to be sufficient to initiate chemical or microbial catalysts. In soil for instance, the type, the sorption capacity or the spatial and energetic distribution of the sorption sites may impose serious limitations on the rate of HOC biotransformation. In order to ensure sufficient transformation rates, environmental biotechnology has to ensure and manage transport of chemicals at least over the distances typically separating hotspots of pollution from transforming microbes (Harms and Wick, 2006). This is of special relevance for HOC which are typically associated with solid particles from which they are very slowly

released by diffusive transport processes (Johnsen et al., 2005; Semple et al., 2007). Using sorbents of either purely mineral or carbonaceous nature, we here suggest that the application of EOF may be used to control PHE-matrix interactions as a driver for subsequent PHE availability to organisms. In natural systems however, sorbent matrices typically consist of a mixture of mineral and carbonaceous materials and may result in hardly predictable benefits of electrokinetic HOC flushing and biodegradation (Gill et al., 2014; Wick et al., 2007) despite of the absence of apparent negative DC-field effects on soil microbial communities (Wick et al., 2010). Knowledge of the composition of environmental matrices and their chemical, thermodynamic and sorption properties is important for the prediction of electrokinetic effects on HOC-matrix interactions. For example, at situations of low organic carbon content (< 1 g kg^{-1}) the mineral phase may dominate and given sufficient electrolyte concentrations DC fields will significantly reduce HOC retention and, hence, increase HOC availability. On the other hand, in activated charcoal treatment of contaminated groundwater or thermal soil remediation technology using activated carbon, DC electric fields may elevate HOC sorption rates, decrease the risk of HOC diffusion, and save the often expensive sorbent materials. Electrokinetic approaches may be further used to kinetically regulate the interaction of sorbates and sorbents in environmental (bio-)technology (Qin et al., 2015a, 2015b; Shan et al., 2018). This kinetic regulation may give rise to future technical applications, which allows regulating sorption processes, for instance in response to fluctuating sorbate concentrations in contaminated water streams, in electro-bioremediation or to avoid unwanted sorption of hydrophobic solutes in technical applications.

Acknowledgements. This work has been performed in the frame of the Helmholtz Alberta Initiative and contributes to research program topic CITE of the Helmholtz Association. Y.S.

404 acknowledges financial support by the China Scholarship Council (CSC). The authors wish
405 to thank Kai Uwe Goss (UFZ) and Ulf Roland (UFZ) for helpful discussions as well as Jana
406 Reichenbach, Rita Remer and Birgit Würz for skilled technical help. We are likewise grateful
407 to Ulf Roland for providing the zeolites and for performing the BET analysis of the sorbents.
408

REFERENCES

Ahn, S., Werner, D., Karapanagioti, H.K., McGlothlin, D.R., Zare, R.N., Luthy, R.G., 2005. Phenanthrene and Pyrene Sorption and Intraparticle Diffusion in Polyoxymethylene, Coke, and Activated Carbon. Environ. Sci. Technol. 39, 6516–6526. https://doi.org/10.1021/es050113o

Ai, L., Jiang, J., 2012. Removal of methylene blue from aqueous solution with self-assembled cylindrical graphene–carbon nanotube hybrid. Chem. Eng. J. 192, 156–163. https://doi.org/10.1016/j.cej.2012.03.056

Bansal, V., Kim, K.-H., 2015. Review of PAH contamination in food products and their health hazards. Environ. Int. 84, 26–38. https://doi.org/10.1016/j.envint.2015.06.016

Cummings, E.B., Griffiths, S.K., Nilson, R.H., Paul, P.H., 2000. Conditions for similitude between the fluid velocity and electric field in electroosmotic flow. Anal. Chem. 72, 2526–2532. https://doi.org/10.1021/ac991165x

Doke, K.M., Khan, E.M., 2013. Adsorption thermodynamics to clean up wastewater; critical review. Rev. Environ. Sci. Biotechnol. 12, 25–44. https://doi.org/10.1007/s11157-012-9273-z

Drost-Hansen, W., 1978. Water at Biological Interfaces - Structural and Functional Aspects. Phys. Chem. Liq. 7, 243–348. https://doi.org/10.1080/00319107808084734

Duan, L., Naidu, R., 2013. Effect of Ionic Strength and Index Cation on the Sorption of Phenanthrene. Water. Air. Soil Pollut. 224. https://doi.org/10.1007/s11270-013-1700-4

Ghosal, P.S., Gupta, A.K., 2015. An insight into thermodynamics of adsorptive removal of fluoride by calcined Ca–Al–(NO3) layered double hydroxide. RSC Adv. 5, 105889–105900. https://doi.org/10.1039/C5RA20538G

Gill, R.T., Harbottle, M.J., Smith, J.W.N., Thornton, S.F., 2014. Electrokinetic-enhanced bioremediation of organic contaminants: a review of processes and environmental applications. Chemosphere 107, 31–42. https://doi.org/10.1016/j.chemosphere.2014.03.019

Harms, H., Smith, K.E.C., Wick, L.Y., 2017a. Problems of Hydrophobicity/Bioavailability: An Introduction, in: Krell, T. (Ed.), Cellular Ecophysiology of Microbe. Springer International Publishing, Cham, pp. 1–13. https://doi.org/10.1007/978-3-319-20796-4_38-1

Harms, H., Wick, L.Y., 2006. Dispersing pollutant-degrading bacteria in contaminated soil without touching it. Eng. Life Sci. 6, 252–260. https://doi.org/10.1002/elsc.200620122

Harms, H., Wick, L.Y., Smith, K.E.C., 2017b. Matrix:Hydrophobic Compound Interactions, in: Krell, T. (Ed.), Cellular Ecophysiology of Microbe. Springer International Publishing, Cham, pp. 1–13. https://doi.org/10.1007/978-3-319-20796-4_39-1

Hassan, I., Mohamedelhassan, E., Yanful, E.K., Yuan, Z.-C., 2015. Sorption of phenanthrene by kaolin and efficacy of hydraulic versus electroosmotic flow to stimulate desorption. J. Environ. Chem. Eng. 3, 2301–2310. https://doi.org/10.1016/j.jece.2015.08.011

Ho, Y.S., Ng, J.C.Y., McKay, G., 2000. Kinetics of pollutant sorption by biosorbents. Sep. Purif. Methods 29, 189–232. https://doi.org/10.1081/SPM-100100009

Hoshyargar, V., Talebi, M., Ashrafizadeh, S.N., Sadeghi, A., 2018. Hydrodynamic dispersion by electroosmotic flow of viscoelastic fluids within a slit microchannel. Microfluid. Nanofluidics 22, 4. https://doi.org/10.1007/s10404-017-2021-5

Huang, W., Weber, W.J., 1997. Thermodynamic considerations in the sorption of organic contaminants by soils and sediments. 1. The isosteric heat approach and its application to model inorganic sorbents. Environ. Sci. Technol. 31, 3238–3243. https://doi.org/10.1021/es970230m

James, G., Sabatini, D.A., Chiou, C.T., Rutherford, D., Scott, A.C., Karapanagioti, H.K., 2005. Evaluating phenanthrene sorption on various wood chars. Water Res. 39, 549–558. https://doi.org/10.1016/j.watres.2004.10.015

Jeon, C.-S., Yang, J.-S., Kim, K.-J., Baek, K., 2010. Electrokinetic Removal of Petroleum Hydrocarbon from Residual Clayey Soil Following a Washing Process. CLEAN - Soil Air Water 38, 189–193. https://doi.org/10.1002/clen.200900190

Johnsen, A.R., Wick, L.Y., Harms, H., 2005. Principles of microbial PAH-degradation in soil. Environ. Pollut. 133, 71–84. https://doi.org/10.1016/j.envpol.2004.04.015

Kim, J.-H., Han, S.-J., Kim, S.-S., Yang, J.-W., 2006. Effect of soil chemical properties on the remediation of phenanthrene-contaminated soil by electrokinetic-Fenton process. Chemosphere 63, 1667–1676. https://doi.org/10.1016/j.chemosphere.2005.10.008

Kim, J.H., Kim, S.S., Yang, J.W., 2007. Role of stabilizers for treatment of clayey soil contaminated with phenanthrene through electrokinetic-Fenton process—Some experimental evidences. Electrochimica Acta 53, 1663–1670. https://doi.org/10.1016/j.electacta.2007.06.082

Kopinke, F.-D., Georgi, A., Goss, K.-U., 2018. Comment on “Mistakes and inconsistencies regarding adsorption of contaminants from aqueous solution: A critical review, published by Tran et al. [Water Research 120, 2017, 88–116].” Water Res. 129, 520–521. https://doi.org/10.1016/j.watres.2017.09.055

Li, A., Cheung, K.A., Reddy, K.R., 2000. Cosolvent-enhanced electrokinetic remediation of soils contaminated with phenanthrene. J. Environ. Eng. 126, 527–533. https://doi.org/10.1061/(ASCE)0733-9372(2000)126:6(527)

Li, H., Wang, Y., Zheng, H., 2018. Variations of moisture and organics in activated sludge during Fe0/S2O82− conditioning–horizontal electro-dewatering process. Water Res. 129, 83–93. https://doi.org/10.1016/j.watres.2017.11.006

Liu, Y., 2009. Is the Free Energy Change of Adsorption Correctly Calculated? J. Chem. Eng. Data 54, 1981–1985. https://doi.org/10.1021/je800661q

Mader, B.T., Uwe-Goss, K., Eisenreich, S.J., 1997. Sorption of nonionic, hydrophobic organic chemicals to mineral surfaces. Environ. Sci. Technol. 31, 1079–1086. https://doi.org/10.1021/es960606g

Morelis, S., van Noort, P.C.M., 2008. Kinetics of phenanthrene desorption from activated carbons to water. Chemosphere 71, 2044–2049. https://doi.org/10.1016/j.chemosphere.2008.01.048

Moustafa, A.M.A., 2009. Fabrication, Characterization and Oil Spill remediation Properties of Exfoliated Graphite (MSc. Dissertation). Pennsylvania State University, University park, PA.

Pham, T.D., Shrestha, R.A., Sillanpää, M., 2009. Removal of hexachlorobenzene and phenanthrene from clayey soil by surfactant-and ultrasound-assisted electrokinetics. J. Environ. Eng. 136, 739–742. https://doi.org/10.1061/(ASCE)EE.1943-7870.0000203

Puglisi, E., Cappa, F., Fragoulis, G., Trevisan, M., Del Re, A.A.M., 2007. Bioavailability and degradation of phenanthrene in compost amended soils. Chemosphere 67, 548–556. https://doi.org/10.1016/j.chemosphere.2006.09.058

Qin, J., Moustafa, A., Harms, H., El-Din, M.G., Wick, L.Y., 2015a. The power of power: Electrokinetic control of PAH interactions with exfoliated graphite. J. Hazard. Mater. 288, 25–33. https://doi.org/10.1016/j.jhazmat.2015.02.008

Qin, J., Sun, X., Liu, Y., Berthold, T., Harms, H., Wick, L.Y., 2015b. Electrokinetic Control of Bacterial Deposition and Transport. Environ. Sci. Technol. 49, 5663–5671. https://doi.org/10.1021/es506245y

Reddy, K.R., 2010. Technical Challenges to In-situ Remediation of Polluted Sites. Geotech. Geol. Eng. 28, 211–221. https://doi.org/10.1007/s10706-008-9235-y

Reddy, K.R., Maturi, K., Cameselle, C., 2009. Sequential electrokinetic remediation of mixed contaminants in low permeability soils. J. Environ. Eng. 135, 989–998. https://doi.org/10.1061/(ASCE)EE.1943-7870.0000077

Reddy, K.R., Saichek, R.E., 2004. Enhanced Electrokinetic Removal of Phenanthrene from Clay Soil by Periodic Electric Potential Application. J. Environ. Sci. Health Part A 39, 1189–1212. https://doi.org/10.1081/ESE-120030326

Rice, C.L., Whitehead, R., 1965. Electrokinetic flow in a narrow cylindrical capillary. J. Phys. Chem. 69, 4017–4024. https://doi.org/10.1021/j100895a062

Saichek, R.E., Reddy, K.R., 2003. Effect of pH control at the anode for the electrokinetic removal of phenanthrene from kaolin soil. Chemosphere 51, 273–287. https://doi.org/10.1016/S0045-6535(02)00849-4

Semple, K.T., Doick, K.J., Wick, L.Y., Harms, H., 2007. Microbial interactions with organic contaminants in soil: Definitions, processes and measurement. Environ. Pollut. 150, 166–176. https://doi.org/10.1016/j.envpol.2007.07.023

Shan, Y., Harms, H., Wick, L.Y., 2018. Electric Field Effects on Bacterial Deposition and Transport in Porous Media. Environ. Sci. Technol. 52, 14294–14301. https://doi.org/10.1021/acs.est.8b03648

Shaplro, A.P., Probstein, R.F., 1993. Removal of contaminants from saturated clay by electroosmosis. Environ. Sci. Technol. 27, 283–291. https://doi.org/10.1021/es00039a007

Sharma, P.K., Rao, K.H., 2003. Adhesion of Paenibacillus polymyxa on chalcopyrite and pyrite: surface thermodynamics and extended DLVO theory. Colloids Surf. B Biointerfaces 29, 21–38. https://doi.org/10.1016/S0927-7765(02)00180-7

Shi, L., Harms, H., Wick, L.Y., 2008. Electroosmotic Flow Stimulates the Release of Alginate-Bound Phenanthrene. Environ. Sci. Technol. 42, 2105–2110. https://doi.org/10.1021/es702357p

Sinton, D., Li, D., 2003. Electroosmotic velocity profiles in microchannels. Colloids Surf. Physicochem. Eng. Asp. 222, 273–283.

Su, Y.-H., Zhu, Y.-G., Sheng, G., Chiou, C.T., 2006. Linear Adsorption of Nonionic Organic Compounds from Water onto Hydrophilic Minerals: Silica and Alumina. Environ. Sci. Technol. 40, 6949–6954. https://doi.org/10.1021/es0609809

Tallarek, U., Rapp, E., Van As, H., Bayer, E., 2001. Electrokinetics in fixed beds: Experimental demonstration of electroosmotic perfusion. Angew. Chem. Int. Ed. 40, 1684–1687. https://doi.org/10.1002/1521-3773(20010504)40:9<1684::AID-ANIE16840>3.0.CO;2-C

Tran, H.N., You, S.-J., Hosseini-Bandegharaei, A., Chao, H.-P., 2017. Mistakes and inconsistencies regarding adsorption of contaminants from aqueous solutions: A critical review. Water Res. 120, 88–116. https://doi.org/10.1016/j.watres.2017.04.014

Vallano, P.T., Remcho, V.T., 2000. Modeling Interparticle and Intraparticle (Perfusive) Electroosmotic Flow in Capillary Electrochromatography. Anal. Chem. 72, 4255–4265. https://doi.org/10.1021/ac0005969

Wick, L.Y., Shi, L., Harms, H., 2007. Electro-bioremediation of hydrophobic organic soil-contaminants: A review of fundamental interactions. Electrochimica Acta 52, 3441–3448. https://doi.org/10.1016/j.electacta.2006.03.117

Wick, L.Y., Buchholz, F., Fetzer, I., Kleinsteuber, S., Hartg, C., Miltner, A., Harms, H., Pucci G.N. 2010. Responses of soil microbial communities to weak electric fields. Sci. Tot. Environ. 408, 4886-4893. https://doi.org 10.1016/j.scitotenv.2010.06.048Zhang, H., Lin, K., Wang, H., Gan, J., 2010. Effect of *Pinus radiata* derived biochars on soil sorption and desorption of phenanthrene. Environ. Pollut. 158, 2821–2825. https://doi.org/10.1016/j.envpol.2010.06.025

Zhao, J., Wang, Z., Zhao, Q., Xing, B., 2014. Adsorption of Phenanthrene on Multilayer Graphene as Affected by Surfactant and Exfoliation. Environ. Sci. Technol. 48, 331–339. https://doi.org/10.1021/es403873r

Table 1. Overview of the properties (BET surface area, pore size and zeta potential (ζ)) of the sorbents used in the study and their temperature-dependent Freundlich sorption isotherm parameters (K_F and n) of PHE sorption at C_e = 400 µg L^{-1} in 10 and 100 mmol L^{-1} electrolyte.

Sorbents	Properties						10 mmol L^{-1}							100 mmol L^{-1}						
	BET Surface (m^2 g^{-1})	Pore Size (nm)	Zeta potential ζ (mV)				5°C		25°C		35°C		25°C	5°C		25°C		35°C		25°C
			1 mM	10 mM	50 mM	100 mM	log K_F [c]	n	Log K_F	n	log K_F	n	K_d* [b]	log K_F	n	log K_F	n	log K_F	n	K_d* [b]
Silica 40Å	675	4	-39.8	-33.3	-22	-18.5	-0.80	0.83	-1.05	0.84	-1.17	0.84	0.0049	-1.05	0.84	-1.34	0.84	-1.58	0.85	0.0026
Silica 60Å	404	6	-35.1	-28.3	-20.3	-17	-1.48	0.83	-1.79	0.84	-1.83	0.84	0.0016	-1.45	0.84	-1.80	0.84	-1.90	0.84	0.0015
Silica 100Å	300	10	-33.5	-25	-22.7	-17.2	-1.66	0.83	-1.83	0.84	-1.88	0.85	0.0019	-1.52	0.84	-1.83	0.84	-1.95	0.84	0.0018
Zeolite NaY	199	2	-43.5	-41.2	-30.8	-25.8	-0.55	0.43	-0.64	0.42	-0.74	0.44	0.00037	-0.45	0.42	-0.65	0.44	-0.81	0.44	0.00049
Zeolite 13X	683	2.1	-47.8	-45.2	-33.8	-28.3	-2.47	0.90	-2.77	0.91	-2.95	0.91	0.00015	-2.03	0.91	-2.30	0.91	-2.53	0.92	0.00043
Al_2O_3	782	3.5	-39.0	-35.5	-28.5	-27.6	-2.85	0.94	-3.25	1.04	-3.00	0.93	0.00092	-2.76	1	-3.02	1.00	-3.09	0.99	0.00097
AC [c]	717	2.8	n.a.[a]	-17	n.a.[a]	-11	1.54	1.96	1.4	2.65	1.20	2.71	0.136	2.16	2.01	1.84	2.16	1.61	3.44	0.148
EG [d]	525	n.a.[a)]	n.a.	-9	n.a.	-5.6	3.67	1.96	3.14	2.12	2.76	2.14	0.133	1.62	1.93	0.74	1.98	0.69	2.09	0.138

[a)] n.a. = not applicable, [b)] surface normalized K_d^* ($\times 10^{-3}$ mL cm^{-2}), [c)] log K_F as (µg kg_{EG}^{-1})(L $\mu g^{-1})^n$, [c)], activated charcoal, [d)] exfoliated graphite.

572 **Table 2.** Table of changes of the Gibbs free energy (ΔG^o), enthalpy (ΔH^o) and the entropy
573 (ΔS^o) of PHE sorbing to different mineral and carbonaceous sorbents at 25 °C in 10 and
574 100 mmol L^{-1} PB electrolyte solutions.
575

Sorbents		10 mmol L^{-1}			100 mmol L^{-1}		
		ΔG^O (kJ mol^{-1})	ΔH^O (kJ mol^{-1})	ΔS^O (kJ mol^{-1} K^{-1})	ΔG^O (kJ mol^{-1})	ΔH^O (kJ mol^{-1})	ΔS^O (kJ mol^{-1} K^{-1})
Mineral Sorbents	**Silica** 40 Å	-11.1	-20.2	-0.03	-9.47	-28.0	-0.06
	Silica 60 Å	-6.9	-20.0	-0.04	-6.85	-25.1	-0.06
	Silica 100 Å	-6.7	-12.3	-0.02	-6.68	-23.7	-0.06
	Zeolite NaY	-13.5	-9.8	0.01	-13.4	-19.0	-0.02
	Zeolite 13X	-1.3	-25.8	-0.08	-3.99	-26.3	-0.07
	Al_2O_3	-4.0	-11.2	0.02	-4.70	-19.1	-0.05
Carbonaceous sorbents	**AC**	-25.1	-36.3	-0.04	-27.6	-29.3	-0.01
	EG	-22.6	-32.2	-0.03	-21.3	-54.0	-0.11

576
577

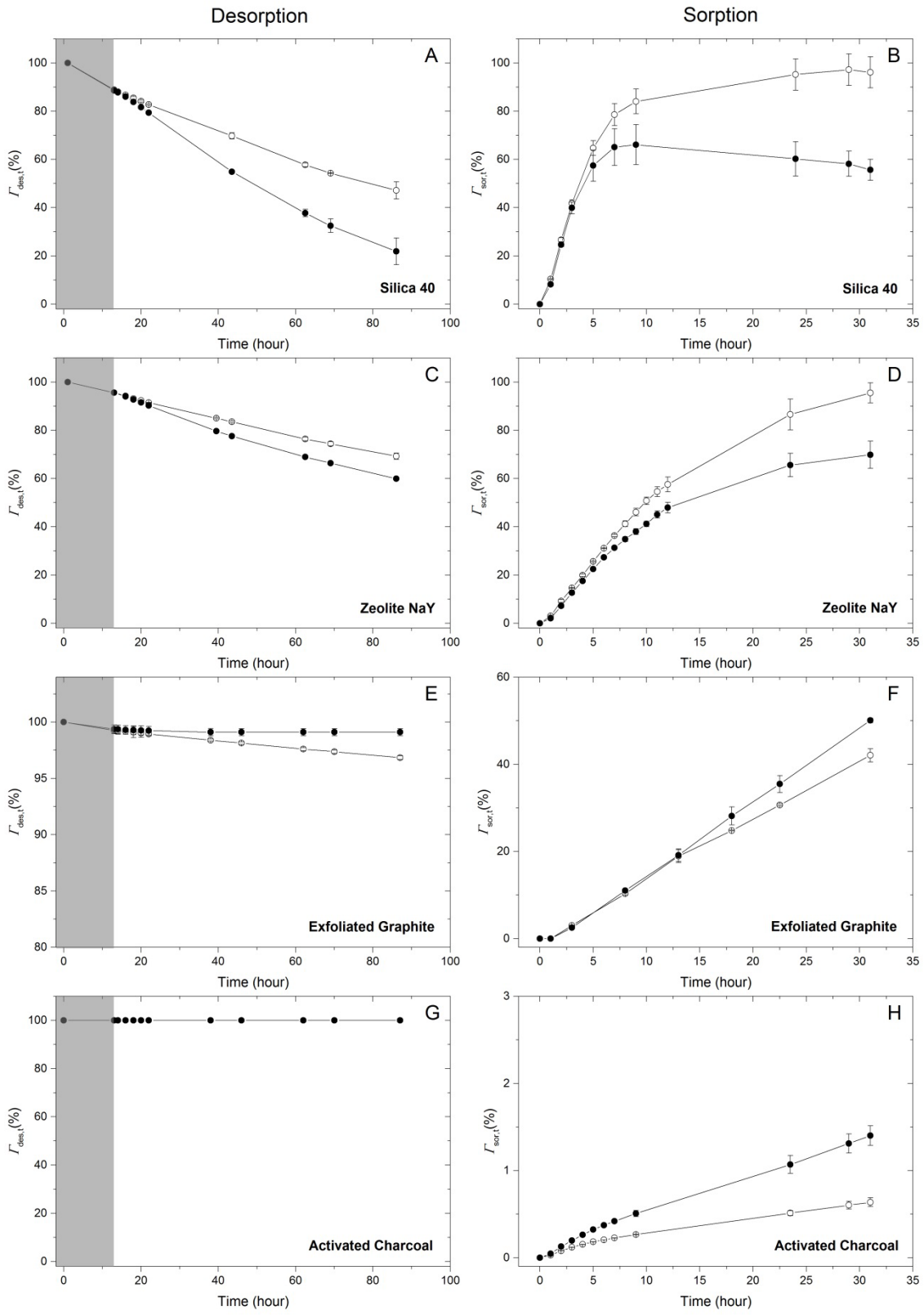
FIGURE LEGENDS

Figure 1. Time dependent normalized PHE fractions in desorption ($\Gamma_{des,t}$) and sorption ($\Gamma_{sor,t}$) experiments in presence (filled symbols) and absence (open symbols) of a DC electric field using a 10 mmol L^{-1} PB electrolyte: silica 40Å (Figures 1A & B), Zeolite NaY (Figures 1C & D), exfoliated graphite (Figures 1E & F), activated charcoal (Figures 1G & H). Areas with a gray background refer to DC-free periods of the experiments. Data represent averages and standard deviations of triplicate experiments.

Figure 2. Effects of PB electrolyte concentrations (1 mmol L^{-1} (squares); 10 mmol L^{-1} (circles), 50 mmol L^{-1} (diamonds) and 100 mmol L^{-1} (triangles)) on the relative DC-induced influence on PHE desorption ($\Delta\Gamma_{des,t}$, Figures 2A, C, E, G) and the DC-induced influence on PHE sorption ($\Delta\Gamma_{sor,t}$, Figures 2B, D, F, H): Silica 40Å (Figures 2A & B), Zeolite NaY (Figures 2C & D), exfoliated graphite (Figures 2E & F), activated charcoal (Figures 2G & H). The grey area refers to no electric field periods. Positive and negative values of $\Delta\Gamma_{des,t}$ refer to increased and reduced desorption in presence of DC, respectively. Positive $\Delta\Gamma_{sor,t}$ denotes decreased sorption to the geo-sorbents relative to the control, while negative values refer to increased sorption. Data represent averages and standard deviations of triplicate experiments.

Figure 3. Effects of the surface normalized partition coefficient K_d^* (Figures 3A & B) and the calculated EOF velocity (Fig 3C & D) on the relative DC-induced PHE desorption benefits ($\Delta\Gamma_{des,t=86\ h}$, Figures 3A & C) and PHE sorption ($\Delta\Gamma_{sor,t=31\ h}$, Figures 3B & D). Circles and triangles refer to mineral and carbonaceous (triangles) sorbents, respectively.

Figure 4. Apparent effects of the calculated electroosmotic flow velocities ($V_{EOF,r}$) and the Gibbs free energy change (ΔG^o) on the relative DC-induced PHE desorption benefits ($\Delta\Gamma_{des,t=86h}$, Figure 4A) and the relative DC-induced PHE sorption benefits ($\Delta\Gamma_{sor,t=31h}$, Figure 4B) using 10 and 100 mmol L^{-1} PB electrolytes.



610

611 **Figure 1**

612

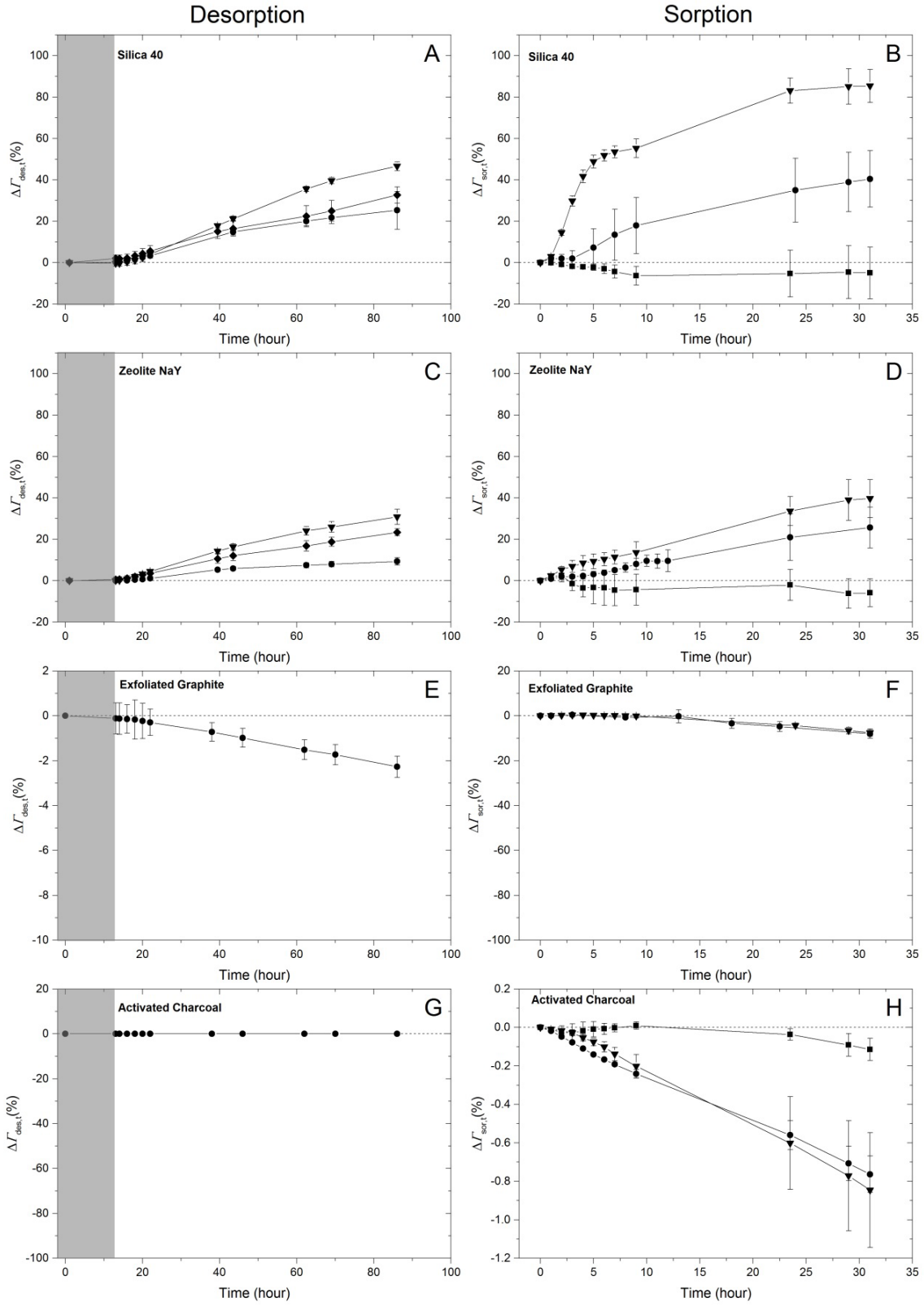
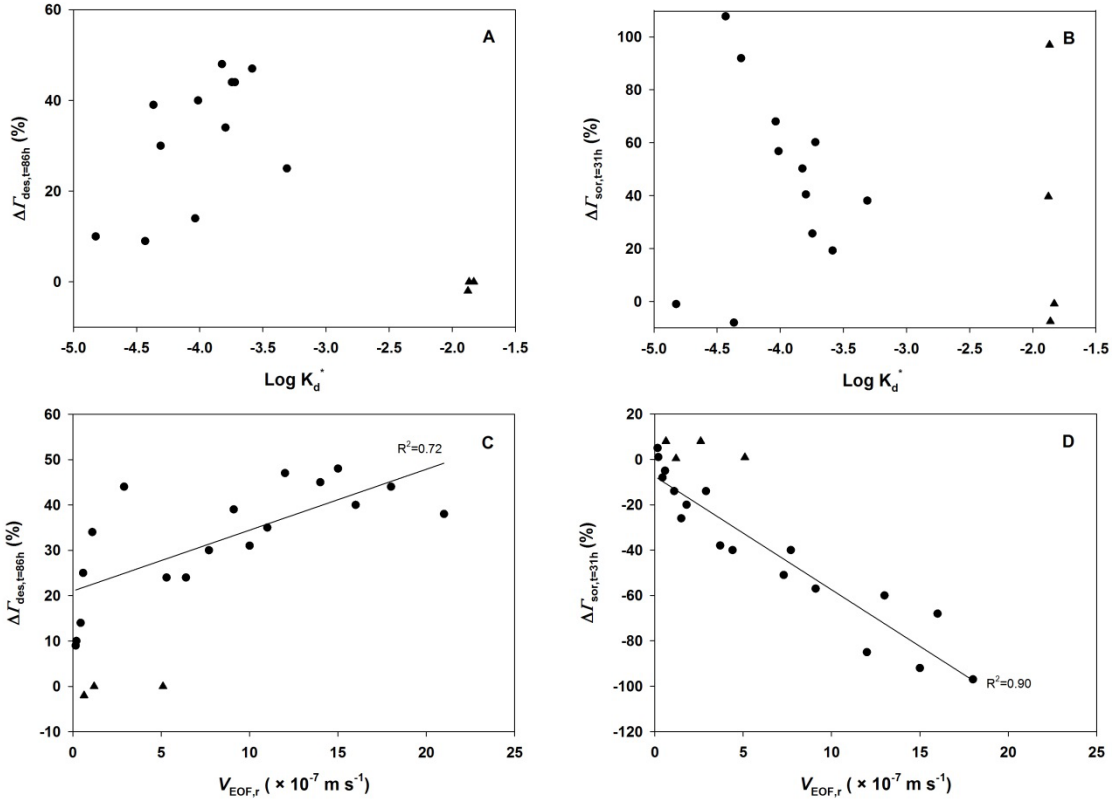

Desorption
Sorption
Silica 40
A
B
Zeolite NaY
C
D
Exfoliated Graphite
E
F
Activated Charcoal
G
H
Time (hour)
$\Delta\Gamma_{des,t}$(%)
$\Delta\Gamma_{sor,t}$(%)

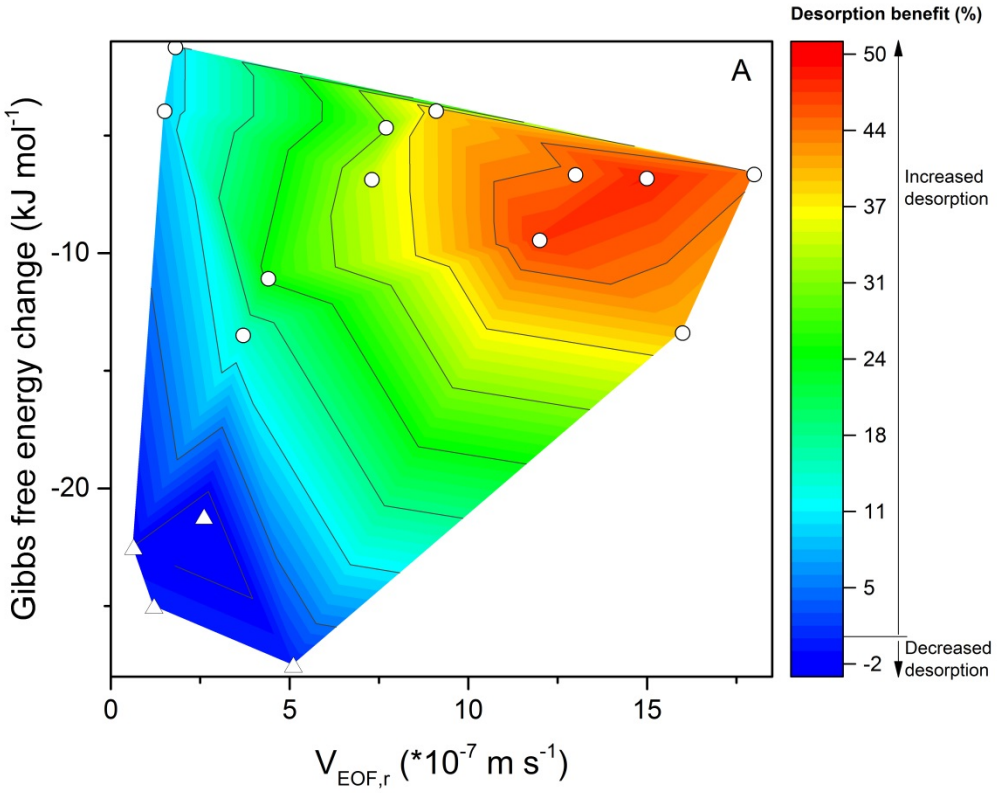
Figure 2



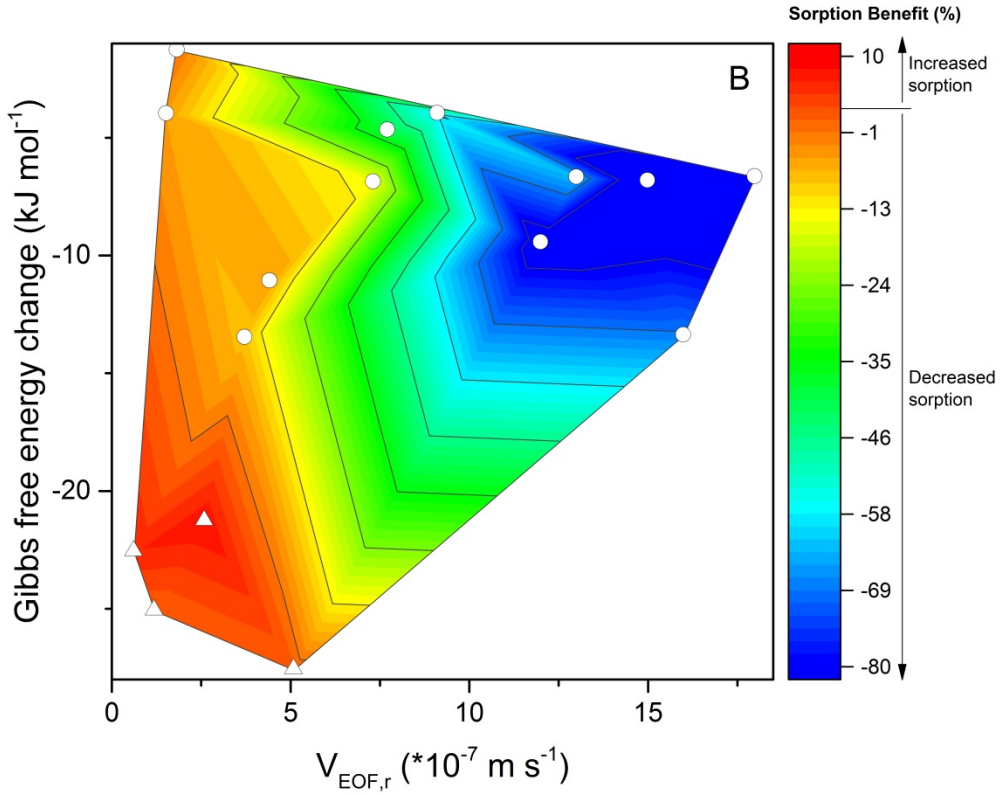
616

617 **Figure 3**

618



619



620 **Figure 4**